

7

Double-interface surface plasmons in symmetric guides

Tables

Item	Topic	Chapter 3	Chapter 4	Chapter 5	Chapter 6	Chapter 7
1	Interfaces	1	1	2	1	2
2	Types	ENG, DNG	DPS, ENG, DNG, MNG	DPS, ENG, DNG, MNG	ENG	ENG
3	ϵ_r, μ_r	complex	real	real	complex	complex
4	Dispersion	yes	no	no	no	no
5	Free β	yes	yes	yes	yes	yes
6	Loaded β	yes	no	no	yes	yes
7	Configuration	O, K	free	free	O, K	G
8	\mathcal{R}	yes	no	no	yes	yes
9	G-H	yes	no	no	no	no
10	E and H	no	yes	yes	yes	yes
11	s_z	no	yes	yes	yes	yes
12	s_x	no	no	no	yes	yes
13	η	yes	no	no	yes	yes
14	v_{ph} and v_{group}	yes	no	no	no	no
15	Charge density	no	no	no	yes	yes

Table 2.10. List of topics investigated in chapters 3-7.

Item	Topic	Chapter 7
1	Interfaces	2
2	Types	ENG
3	ϵ_r, μ_r	complex
4	Dispersion	no
5	Free β	yes
6	Loaded β	yes
7	Configuration	G
8	\mathcal{R}	yes
9	G-H	no
10	E and H	yes
11	S_z	yes
12	S_x	yes
13	η	yes
14	v_{ph} and v_{group}	no
15	Charge density	yes

Table 7.1. List of topics investigated in this chapter.

	ϵ_i	μ_i	n_i	r_i	ϕ_i
Prism	6.25	1.	2.5		
Cover	2.25	1.	1.5	2.46221	0.418224
Metal	-15.9958 + 0.52 i	1.	0.0649999 + 4. i	16.027	3.07916
Substrate	2.25	1.	1.5	2.46221	0.418224

Table 7.2. The value of ϵ_i , μ_i , n_i , r_i and ϕ_i belonging to the prism, cover, guide and substrate.

	Long-range mode	Short-range mode
β	1.51928 + 0.000218585 i	2.12771 + 0.0335961 i
δ	0.241266 + 0.00137645 i	1.50939 + 0.0473587 i
κ	0.0606878 + 4.27875 i	0.0416126 + 4.53029 i
γ	0.241266 + 0.00137645 i	1.50939 + 0.0473587 i

Table 7.3. The solution of the complex mode equation, for $d_m = 20$ nm, yields the complex values of β , δ , κ and δ , each for the SR and LR modes.

	System	ζ (μm)	N_ζ (cycles)	τ_ζ (fs)
(a) PW	silver	0.0251783	0.01625	0.00545907
(b) SR	glass/silver/glass	2.99776	63.3319	21.2759
(c) MR	glass/silver	23.4248	376.32	126.422
(c) LR	glass/silver/glass	460.751	6950.51	2334.98

Table 7.4. The 1/e propagation distance, ζ , the number of wave cycles per decay length, N_ζ , and the lifetime, τ_ζ , for a plane wave (PW) incident normal to a thick silver film, and for SR, MR and LR modes.

Mode	C
LR	137.653
SR	292.098

Table 7.5. The normalization constant, C , of the fields associated with a power of one W per one meter width of the guide for the LR and SR modes.

	η_i/η_0	η_{LR}/η_0	η_{SR}/η_0
Cover	0.666667	$0.675235 + 0.000097149 i$	$0.945648 + 0.0149316 i$
Metal	$0.00406142 - 0.249934 i$	$-0.0948791 - 0.00309805 i$	$-0.132808 - 0.0064177 i$
Substrate	0.666667	$0.675235 + 0.000097149 i$	$0.945648 + 0.0149316 i$

Table 7.6. The relative wave impedance of the bulk media and the LR and SR modes, η_i/η_0 , η_{LR}/η_0 and η_{SR}/η_0 , respectively, where η_0 is the free space impedance and i denotes substrate, metal and cover.

Mode	$P_{c,z}$	$P_{m,z}$	$P_{s,z}$	P_z
LR	0.503018	-0.00603836	0.503018	1
SR	0.50704	-0.0138565	0.50704	1

Table 7.7. The total power flow along the z -direction, $P_{c,z}$, $P_{m,z}$ and $P_{s,z}$, in the cover, guide and substrate, respectively, and their sum, P_z , are obtained by integrating their respective shaded areas as depicted in Fig. 7.14.

Mode	$P_{c,x}$	$P_{s,x}$	P_x
LR	-0.503018	0.503018	0
SR	-0.50704	0.50704	0

Table 7.8. The total power flow along the x -direction, $P_{c,x}$ and $P_{s,x}$, in the cover and substrate, respectively, and their sum, P_x .

n_e ($1/\mu\text{m}^2$)	$x = 0$	$x = -d$
LR	-2.20702	2.20702
MR	-3.63639	
SR	-6.55825	-6.55825

Table 7.9. The peak number of charges n_e at the top ($x = 0$) and bottom ($x = -d_m$) interfaces of the guide for the LR and SR modes and at the top for a single-interface structure (MR). Note the sign of the charges for these two modes.

Mode	β	θ_p (deg)	Γ_p (deg)
LR	$1.51928 + 0.000218585 i$	37.4242	0.00630807
SR	$2.12771 + 0.0335961 i$	58.2993	1.4651

Table 7.10. The complex propagating constants of the LR and SR modes from which the angle of incidence inside the prism, θ_p , and Lorentzian width, Γ_p , are derived.

Figures

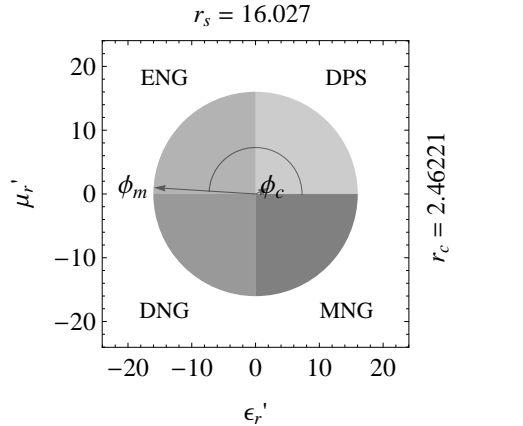


Fig. 7.3. The configuration of the DPS/ENG/DPS-type structure in an ϵ_r' - μ_r' parameter space using the parameters of Table 7.2. Note that here the vectors associated with the cover (and substrate) and guide are in the DPS and ENG quadrants, as expected, yet they differ in their length.

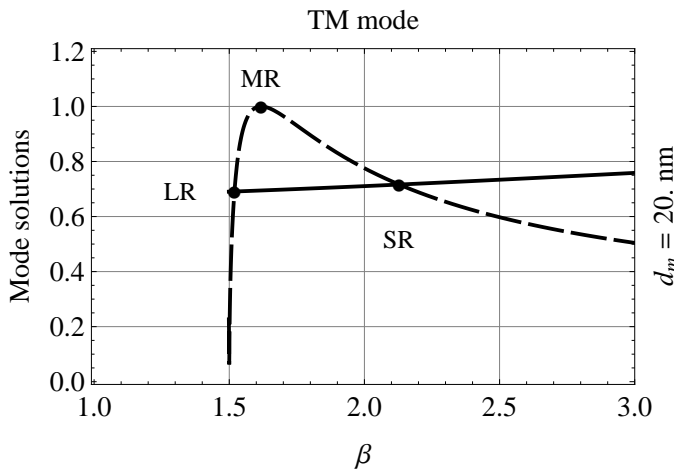


Fig. 7.4. The solution of the approximate TM mode equation is obtained by the intersections of its left-hand side (LHS) and right-hand side (RHS) parts. The two intersections yield the propagation constants, β , of the LR and SR modes which converge to the propagation constant of a single-interface mode, shown by the solid dot denoted by MR, as d_m diverges.

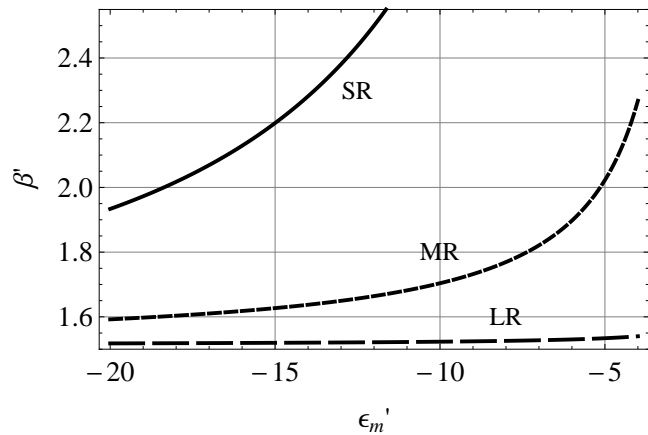


Fig. 7.5. The real part of the propagation constant, β' , as a function of a real-valued, negative permittivity of the guide, ϵ_m' . The solid, dashed and dotted lines refer to β_{SR}' , β_{LR}' and the single interface mode, β_{MR}' , respectively.

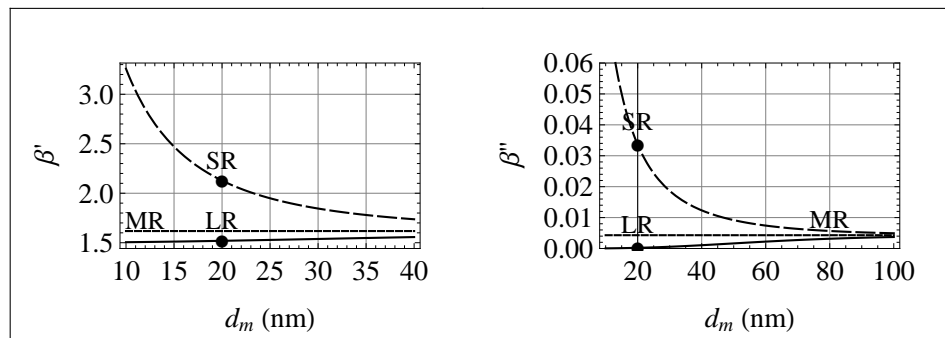


Fig. 7.6. The real and imaginary components of the propagation constant, β' (left) and β'' (right) for the LR, MR and SR modes as a function of the guide thickness, d_m .

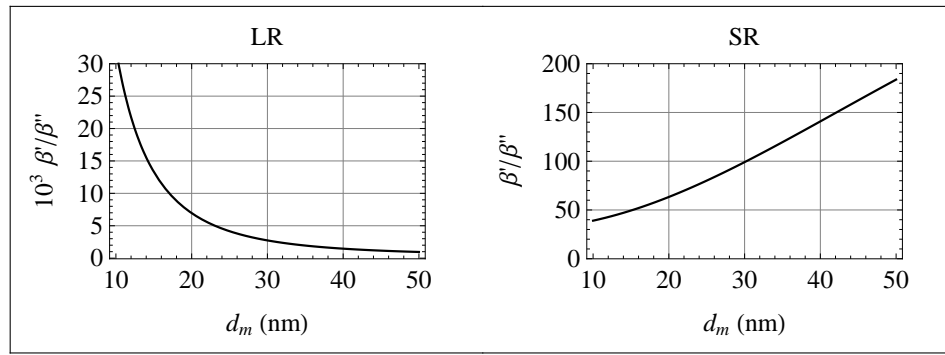


Fig. 7.7. The ratio of the real and imaginary parts of the propagation constant, β'/β'' , for the (left) LR and (right) SR modes as a function of d_m , yields their number of wave cycles per decay length.

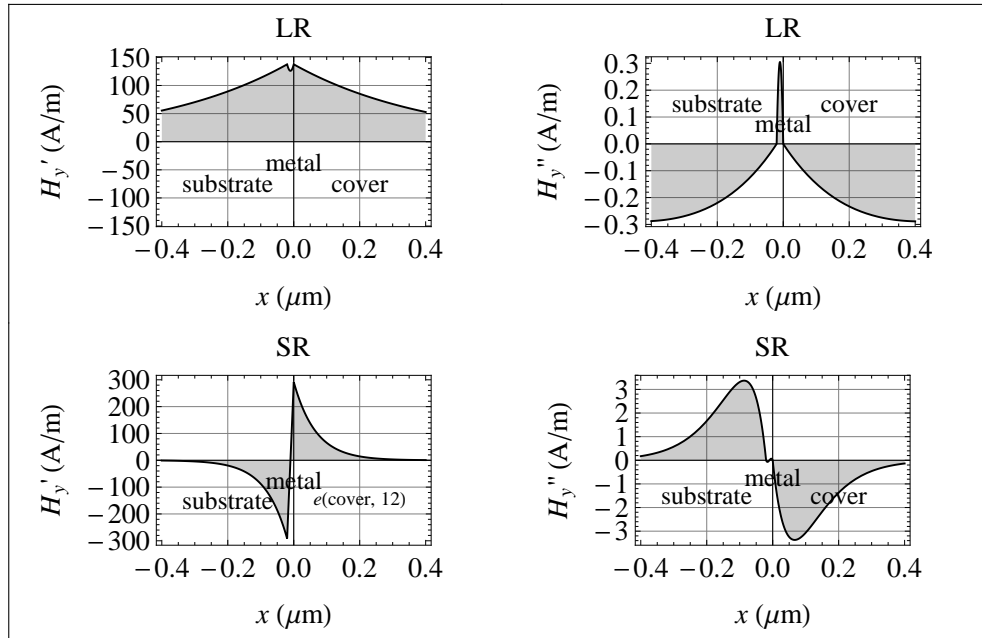


Fig. 7.8. The real and imaginary parts of the magnetic field, H_y' and H_y'' , respectively, for the LR and SR modes as a function of x .

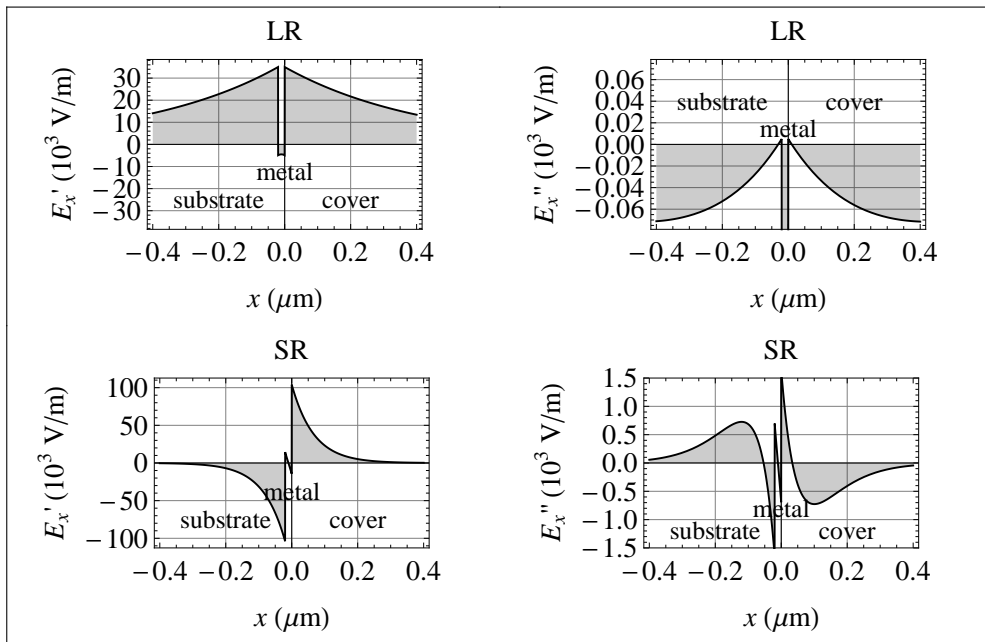


Fig. 7.9. The real and imaginary parts of the electric field, E_x' and E_x'' , respectively, for the LR and SR modes as a function of x .

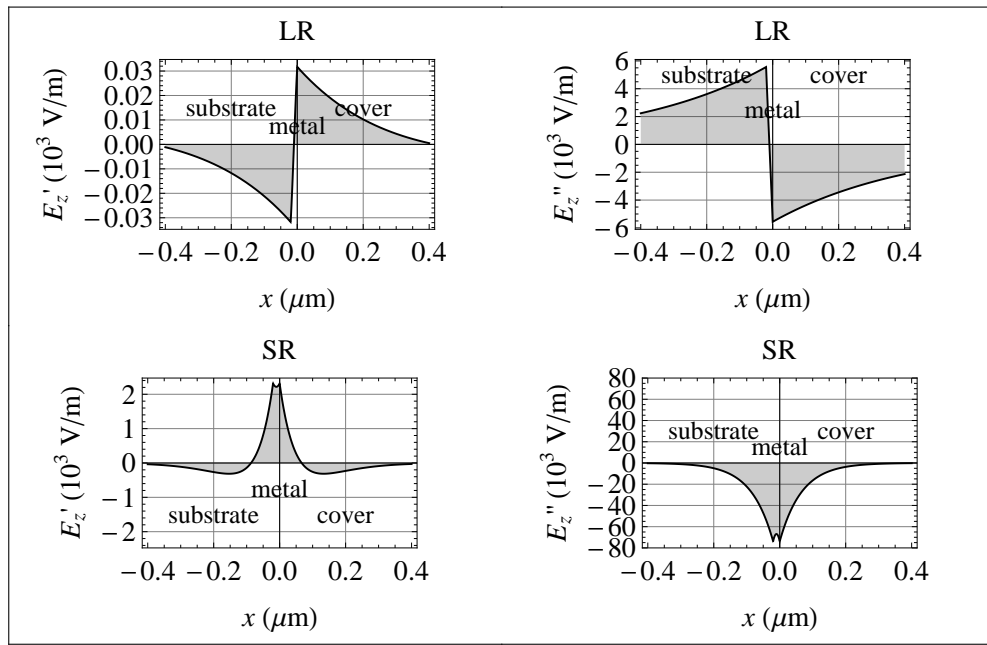


Fig. 7.10. The real and imaginary parts of the electric field, E_z' and E_z'' , respectively, for the LR and SR modes as a function of x .

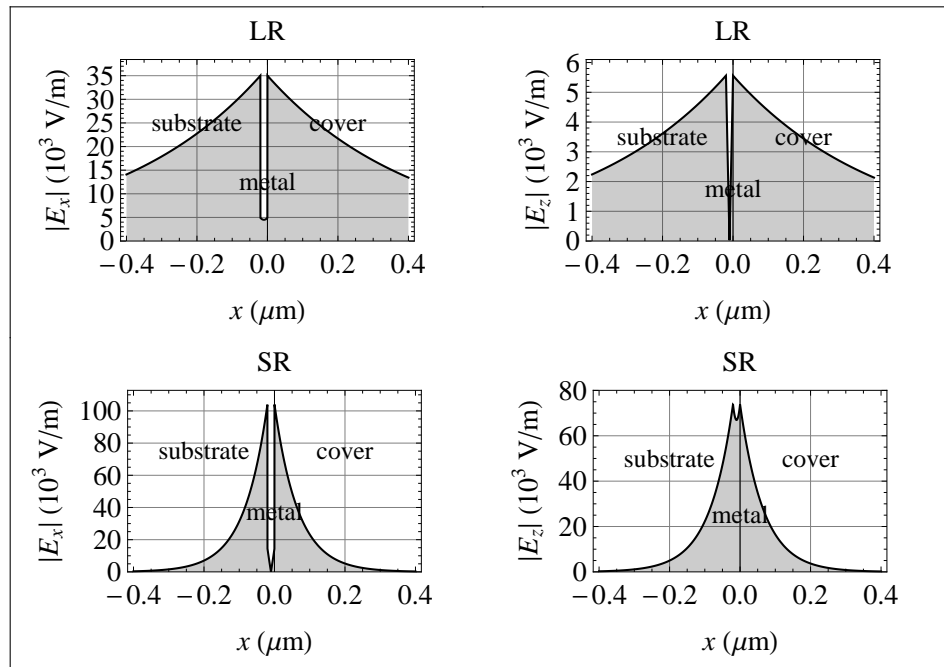


Fig. 7.11. The absolute value of the electric fields, $|E_x|$ and $|E_z|$, for the LR and SR modes as a function x .

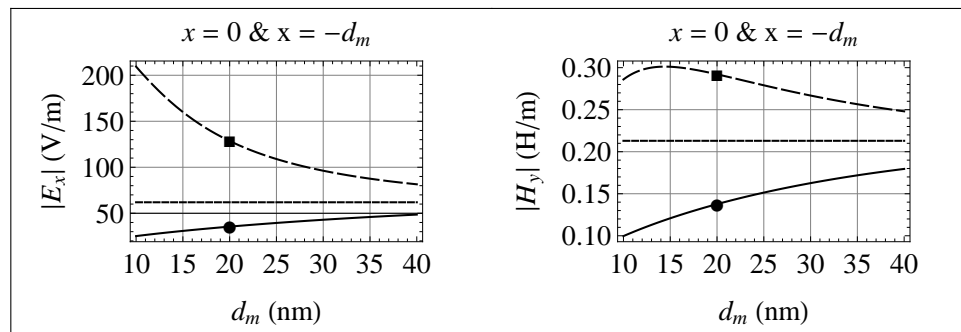


Fig. 7.12. The absolute value of the (left) electric and (right) magnetic field components, $|E_x|$ and $|H_y|$, respectively, at $x = 0$, as a function of the guide thickness, d_m .

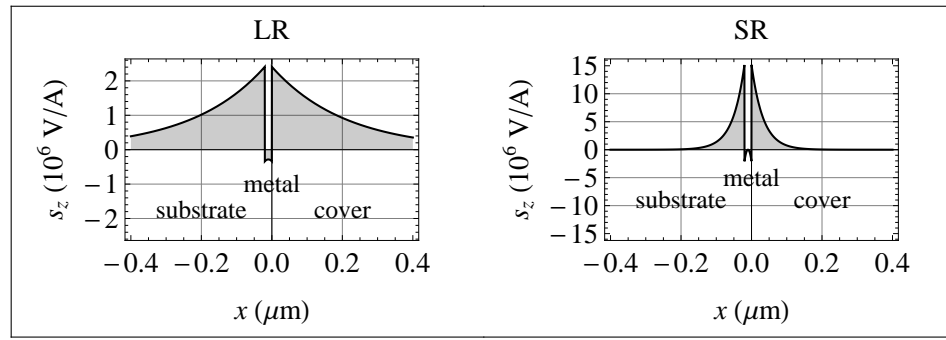


Fig. 7.14. The local power flow along the propagation direction, s_z , associated with the LR and SR modes as a function of x .

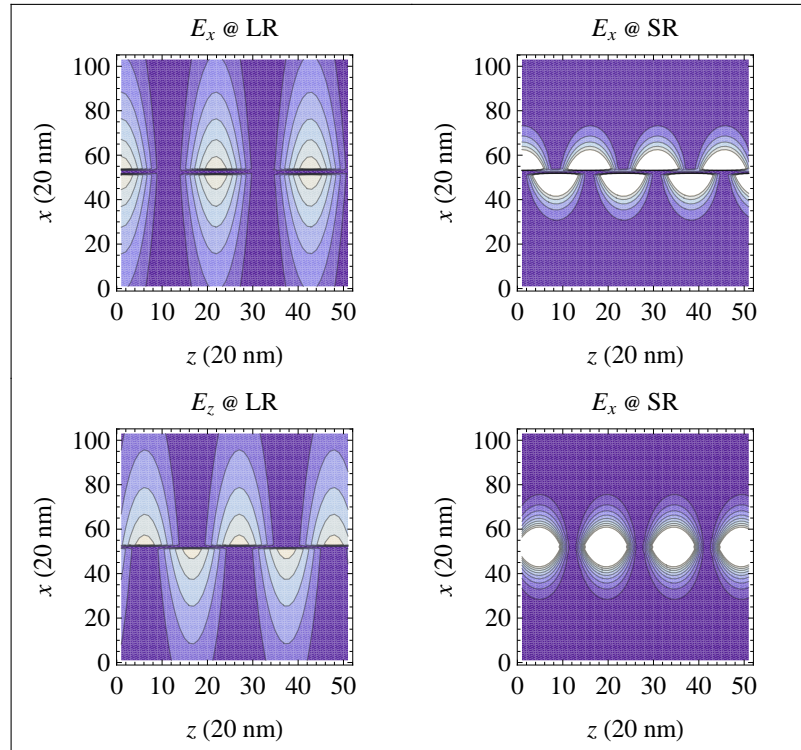


Fig. 7.15. The fields E_x and E_z as functions of x and z for the LR and SR modes in arbitrary units.

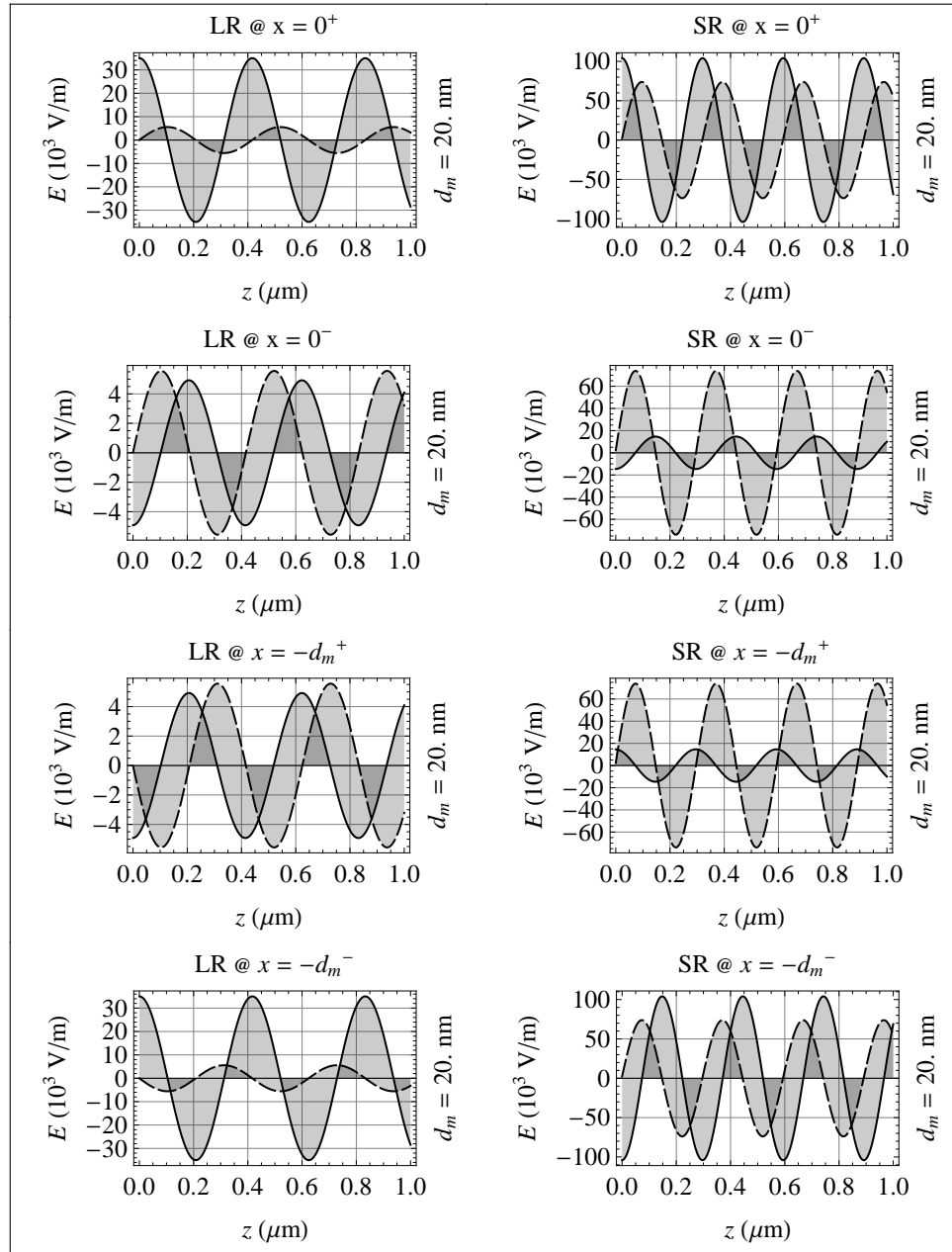


Fig. 7.16. The amplitude and phase of the fields E_x (solid line) and E_z (dashed line) for the LR and SR modes at four points across the guide for $d_m = 20 \text{ nm}$.

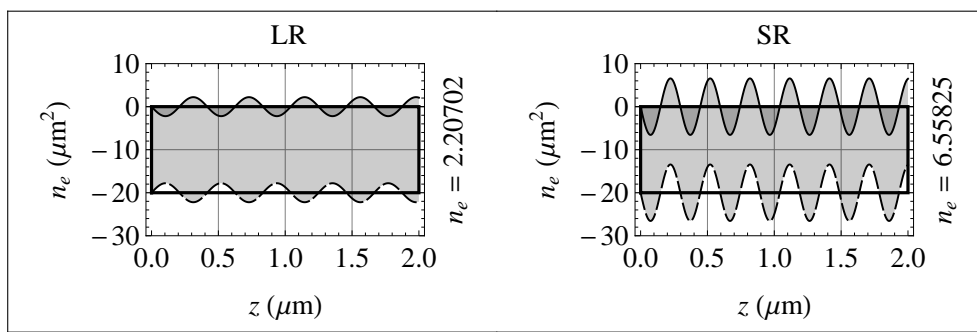


Fig. 7.17. The surface charge density wave across the top and bottom interfaces of the guide for the LR and SR modes showing that they are antisymmetric and symmetric, respectively.

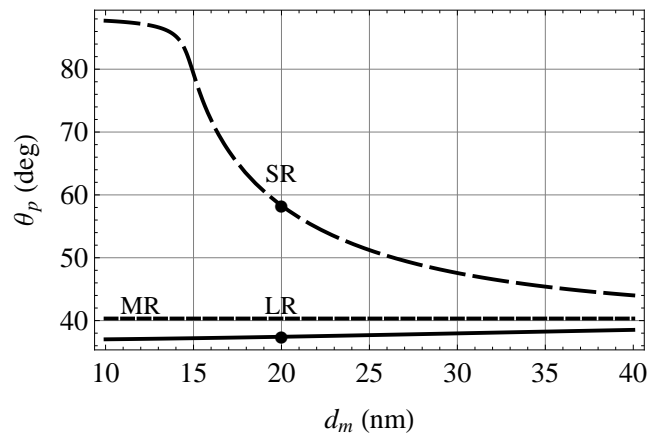


Figure 7.19. The angle θ_p in the prism for the LR, SR and MR mode as a function of the guide thickness, d_m .

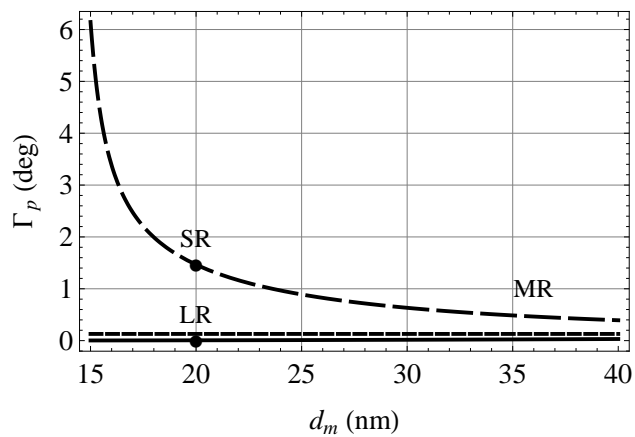


Fig. 7.20. Γ_p as a function of d_m calculated from the complex propagation constants of the LR, SR and MR modes.

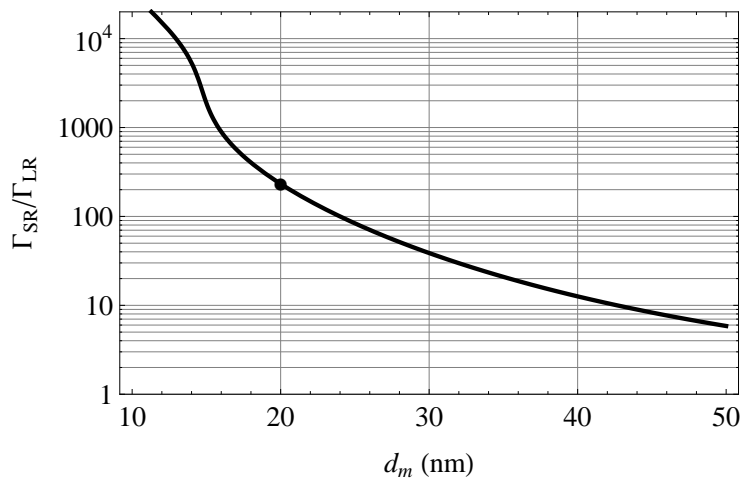


Fig. 7.21. The ratio of the widths Γ_{SR}/Γ_{LR} as a function of d_m calculated from the complex propagation constants of the LR and SR modes.

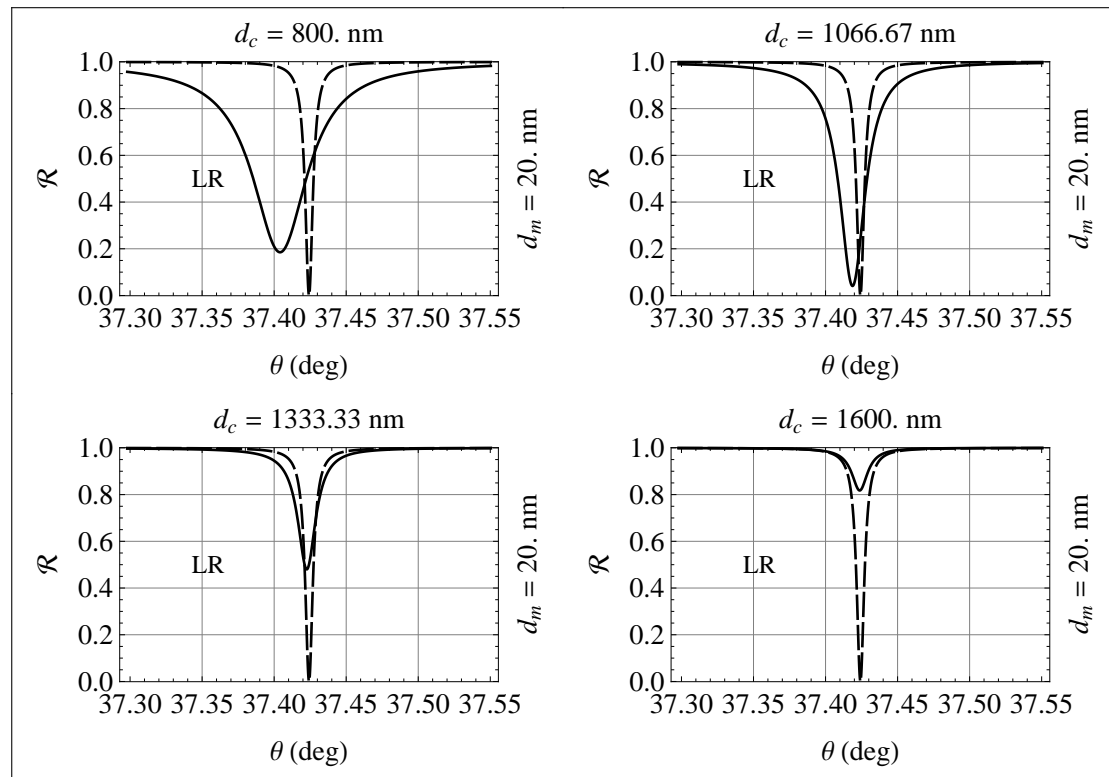


Fig. 7.22. The \mathcal{R} -spectrum (solid line) and Δ -spectrum (dashed line) of the LR mode for a constant guide thickness of $d_m = 20 \text{ nm}$ and cover thicknesses of $d_c = 800, 1,066.67, 1,333.33$ and $1,600 \text{ nm}$.

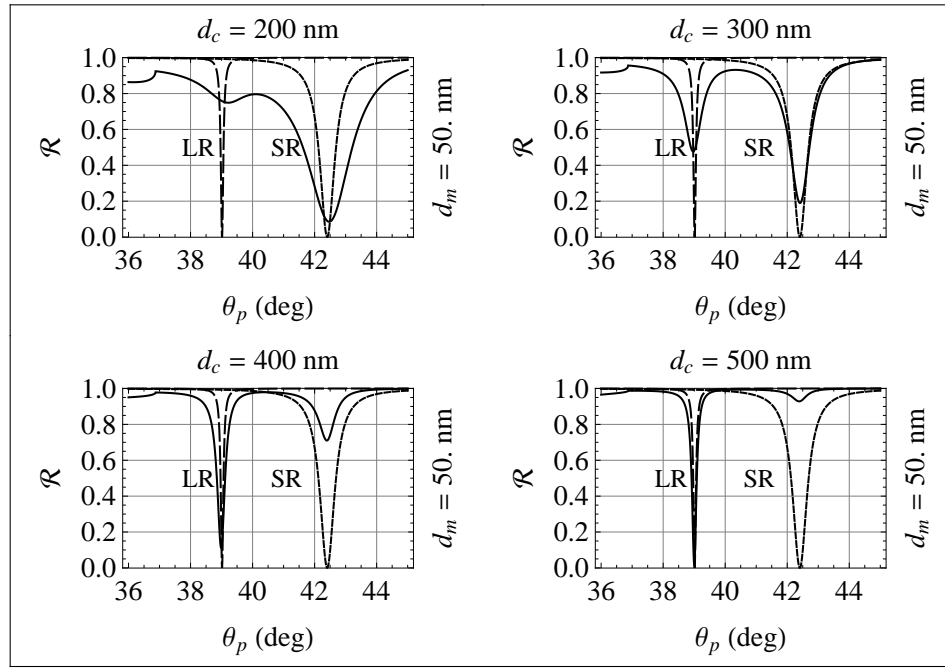


Fig. 7.23. The \mathcal{R} -spectra (solid line) and Δ -spectra (dashed line) of the LR and SR modes for a constant guide thickness of $d_m = 50$ nm and cover thicknesses of $d_c = 200, 300, 400$ and 500 nm.

Exercises

- (1) Complete the missing items in Table 7.1 by developing the code, generating figures and discussing them.
- (2) Compare the advantages and disadvantages of using the general prism coupling configuration relative to the Otto and the Kretschmann configurations.

References

- [1] H. Raether. Excitation of Plasmons and Interband Transitions by Electrons (Springer Tracts in Modern Physics, Vol. 88, Berlin Heidelberg New York, Springer-Verlag, 1980).
- [2] V. M. Agranovich and D. L. Mills, Eds. Surface Polaritons, Electromagnetic Waves at Surfaces and Interfaces (New York, North Holland, 1982).
- [3] A. D. Boardman, Ed. Electromagnetic Surface Modes (New York, John Wiley & Sons, 1982).
- [4] H. Raether. Surface Plasmons on Smooth and Rough Surfaces and on Gratings (Springer Tracts in Modern Physics, Vol. 111, New York, Springer-Verlag, 1988).
- [5] M. Fukui, V. C. Y. So and R. Normandin. Lifetimes of surface plasmons in thin silver films. *Phys. Stat. Sol. (b)* 91 (1979) K61.
- [6] D. Sarid. Long-range surface-plasma waves on very thin metal films. *Phys. Rev. Lett.* 47 (1981) 1927.
- [7] A. E. Craig, G. A. Olson and D. Sarid. Experimental observation of the long-range surface-plasmon polariton. *Opt. Lett.* 8 (1983) 380.
- [8] P. Berini, R. Charbonneau and N. Laboud. Long-Range surface plasmons on ultrathin membranes. *Nano Lett.* 7 (2007) 1376.
- [9] M. Mansuripur, A. R. Zakharian and J. V. Moloney. Surface plasmon polaritons on metallic surfaces. *OPN* 18 (2007) 44.
- [10] R. Charbonneau, E. Lisicka-Shrzek and P. Berini. Broadside coupling to long-range surface plasmons using an angle-cleaved optical fiber. *Appl. Phys. Lett.* 92 (2008) 101102.
- [11] A. Degiron, P. Berini and D. R. Smith. Guiding light with long-range plasmons. *OPN* 19 (2008) 29.